

# Residual Connections Harm Self-Supervised Abstract Feature Learning

Xiao Zhang<sup>1\*</sup>   Ruoxi Jiang<sup>1\*</sup>   William Gao<sup>1</sup>  
Rebecca Willett<sup>1,2</sup>   Michael Maire<sup>1</sup>

<sup>1</sup> Department of Computer Science, The University of Chicago

<sup>2</sup> Department of Statistics, The University of Chicago

**Abstract.** We demonstrate that adding a weighting factor to decay the strength of identity shortcuts within residual networks substantially improves semantic feature learning in the state-of-the-art self-supervised masked autoencoding (MAE) paradigm. Our modification to the identity shortcuts within a ViT-B/16 backbone of an MAE boosts linear probing accuracy on ImageNet from 67.3% to 72.3%. This significant gap suggests that, while residual connection structure serves an essential role in facilitating gradient propagation, it may have a harmful side effect of reducing capacity for abstract learning by virtue of injecting an echo of shallower representations into deeper layers. We ameliorate this downside via a fixed formula for monotonically decreasing the contribution of identity connections as layer depth increases. Our design promotes the gradual development of feature abstractions, without impacting network trainability. Analyzing the representations learned by our modified residual networks, we find correlation between low effective feature rank and downstream task performance.

## 1 Introduction

Residual networks (ResNets) [24] define a connection structure that has achieved near-universal adoption into modern architectures for deep learning. At the time of their development, supervised learning (*e.g.*, ImageNet [15] classification) was the driving force behind the evolution of convolutional neural network (CNN) architectures. Residual networks solved a key issue: CNNs constructed of more than approximately 20 convolutional layers in sequence became difficult to train, leading to shallower networks outperforming deeper ones, unless additional techniques, such as auxiliary outputs [61] or batch normalization [32], were employed. Both ResNets, and their predecessor, highway networks [59] provide elegant solutions to this trainability problem by endowing the network architecture with alternative shortcut pathways along which to propagate gradients. Highway networks present a more general formulation that modulates these shortcut connections with learned gating functions. However, given their sufficient empirical effectiveness, the simplicity of ResNet’s identity shortcuts (residual connections) makes them a preferred technique.

---

\* Equal contribution

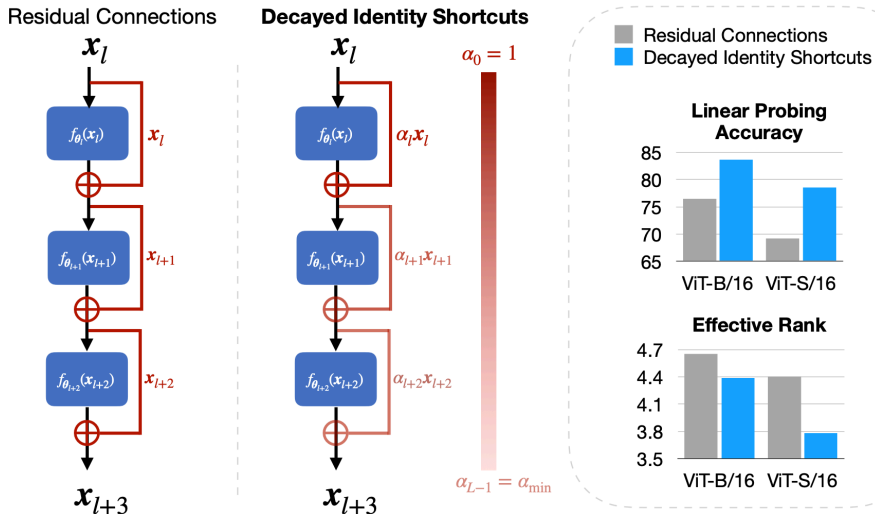


**Fig. 1:** We propose *decayed identity shortcuts*, a variant of standard residual connections, to facilitate self-supervised feature representation learning. Our design introduces a depth-dependent scaling factor to shortcuts in the residual network, which modulates the contribution of preceding layers and fosters greater abstraction in deeper layers. Implementing our design in a Masked Autoencoder (MAE) [26], we show a substantial improvement in feature quality when benchmarking linear probing accuracy on the ImageNet-100 dataset, achieved without the introduction of additional trainable parameters. We further validate our design in terms of feature abstraction by demonstrating that it reduces the effective rank (defined in Section 5) of the output features.

While solving the gradient propagation issue, residual connections impose a specific functional form on the network; between residual connections, each layer (or block of layers) learns to produce an update slated to be added to its own input. This incremental functional form may influence the computational procedures learned by the network [22]. Alternatives to residual and highway networks exist that do not share this functional form, but implement other kinds of skip-connection scaffolding in order to assist gradient propagation [29, 41, 66]. Thus, shortcut pathways, rather than a specific form of skip connection, are the essential ingredient to enable the training of very deep networks. Nevertheless, nearly all modern large-scale models, including those based on the transformer architecture [63] incorporate the standard identity shortcut residual connection.

This design choice holds, even as deep learning has shifted into an era driven by self-supervised training. The shift to self-supervision brings to the forefront new learning paradigms, including those based on contrastive [8, 9, 23, 25, 64], generative [21, 27, 36, 49, 56, 58], and autoencoding [26, 38, 43] objectives. Many systems in the generative and autoencoding paradigms rely on “encoder-decoder” architectures, often styled after the original U-Net [50], which contains additional long-range shortcuts between corresponding layers in mirrored symmetry about

a central bottleneck. With representation learning as a goal, one typically desires that the middle bottleneck layer produce a feature embedding reflecting abstract semantic properties. The interaction of skip-connection scaffolding for gradient propagation with encoder-decoder architectures, self-supervised training objectives, and bottleneck representations has not been carefully reconsidered. This is a worrisome oversight, especially since even in the supervised setting with standard classification architectures, prior work suggests that unweighted identity shortcuts may be a suboptimal design decision [18, 52].

Intuitively, identity shortcut connections may not be entirely appropriate for capturing high-level, semantic representations as they directly inject low-level, high-frequency details of inputs into outputs, potentially compromising feature abstraction. Our work explores this issue within the Masked Autoencoder (MAE) framework of He et al. [26], one of the leading paradigms for self-supervised image representation learning. We demonstrate that identity shortcuts significantly harm semantic feature learning in comparison to an alternative we propose: gradually decay the weight of the identity shortcut over the depth of the network, thereby reducing the information flowing through it (Figure 1). With increasing layer depth, our approach facilitates a smooth transition from a residual to a feed-forward architecture, while maintaining sufficient connectivity to train the network effectively. Unlike prior work on learned gating [59] or reweighting [52] mechanisms for residual connection, our method is a forced decay scheme governed by a single hyperparameter; Section 3 provides details.

Section 4 shows that implementing our novel design within an MAE yields a substantial performance boost in linear probing on ImageNet-1K [15] (72.3% from a baseline 67.3%). Ablation studies on ImageNet-100 show that smaller models equipped with our decayed identity shortcuts can outperform larger ones equipped with standard residual connections. In particular, a ViT-S/16 model [17] with our design outperforms a baseline ViT-B/16 (78.5% *vs.* 76.5%).

A parallel motivation for our design stems from Huh et al. [31], who show that features from residual blocks have higher rank than those produced by comparative feed-forward blocks. The smooth transition between residual and feed-forward behavior induced by our decay scheme should regularize deeper features toward exhibiting low-rank characteristics. Section 5 experimentally explores the correlation between our decayed identity shortcuts and low-rank feature representations. In the self-supervised MAE setting, as well as a supervised learning context, we validate that our method not only improves classification accuracy but also yields low-rank features with distinct cluster structure.

## 2 Related Work

**Self-supervised representation learning.** Recent advancements [1, 39, 48, 49, 54, 62] in deep learning follow a common scaling law, in which a model’s performance consistently improves with its capacity and the size of the training data. This effect can be observed in large language models (LLMs), which are trained on vast amounts of internet text, enabling them to perform some tasks at

human level [42] and exhibit remarkable zero-shot capabilities [40]. These models are trained using next-token-prediction, allowing them to be trained without labeled data. In contrast, the progress of this scaling law in computer vision has largely depended on annotated data. For instance, the Segment Anything model [39] leverages 1 billion human-annotated masks, and state-of-the-art image generators [48] require training on huge datasets of text-image pairs [53]. However, the vast volume of unlabeled visual data and desire for continued scaling motivates a transition to self-supervised learning.

At present, two families of approaches to self-supervised visual representation learning appear particularly promising: contrastive learning [8, 9, 23, 25, 64], which trains a discriminative model to maximize mutual information across image augmentations, and masked image modeling [5, 13, 26], which trains a generative model to predict occluded pixels. Hybrid approaches [30, 43, 65] combine both methods. Despite advancements, neither approach has demonstrated the same scalability [55] as seen in LLMs. This challenge is additional motivation for reconsidering the foundations of self-supervised network architectures.

**Residual and skip-connection architectures.** Highway networks [22] first propose an additive skip connection structure to provide a scaffolding for gradient propagation when training very deep (*e.g.*, 100 layer) networks. Motivated by the gating mechanisms within LSTMs [28], this solution uses learned gating functions to weight each combination of identity and layer output branches. Residual networks [24] are a simplification that removes these learned coefficients. DenseNet [29] and FractalNet [41] demonstrate that access to gradient paths of multiple lengths are the core requirement of training scaffolding, by introducing skip-connection structures with other functional forms. DenseNet utilizes feature concatenation instead of addition, while FractalNet imposes a recursive tree-like architecture combining subnetworks of multiple depths.

Zhu et al. [67] explore variants of ResNets and DenseNets with fewer points of combination between different internal paths, demonstrating that a sparser scaffolding structure may be more robust as network depth increases to thousands of layers. Savarese and Figueiredo [52] add a scalar gating functional to the layer output in residual networks, yielding a hybrid design between residual and highway networks; learning this scalar gating provides a consistent benefit to classification accuracy. Fischer et al. [18] develop a weighting scheme for residual connections based upon a sensitivity analysis of signal propagation within a ResNet. To date, none of these potential improvements have seen broad adoption.

**Low rank bias in neural networks.** Over-parameterized neural networks exhibit surprising generalization capabilities, a finding seemingly in contradiction with classical machine learning theory [45]. This phenomenon implies the existence of some form of implicit regularization that prevents the model from overfitting. From the perspective of neural network parameterizations, Arora et al. [2] suggest that linear models with more layers tend to converge to minimal norm solutions. In the context of CNNs, Huh et al. [31] demonstrates that stacking more feed-forward layers compels the model to seek solutions of a lower rank, and Jing et al. [33] reinforce this finding by adding more layers to an Au-

toencoder’s bottleneck, thereby creating a representation bottleneck. In vision transformers, Geshkovski et al. [19] examine the connection between attention blocks and mean-shift clustering [14], showing that repeated attention operations result in low-rank outputs. Moreover, Dong et al. [16] reveal that eliminating the shortcut connection from residual attention blocks causes features to degenerate to rank 1 structures doubly exponentially. From a different perspective, recent works [6, 46, 47] show training algorithms implicitly induce low-rank behavior in neural networks. Radhakrishnan et al. [47] study the dimensionality reduction behavior of a recursive feature machine [46] and effectively verify performance on low-rank matrix recovery.

### 3 Method

Prior works show that deeper feed-forward architectures have an inductive bias towards producing low-rank feature maps, while ResNets do not display the same behavior [31]. However, despite this bias, deeper feed-forward architectures are typically less effective and generalize worse than ResNets [24]. We aim to combine the properties of both feed-forward networks and ResNets, using the low-rank prior to enhance the abstraction capability of the network while maintaining the core benefits of the residual block, including stable training and the capacity to construct deeper models.

#### 3.1 Decayed Identity Shortcuts

**Feed-forward layers.** Consider a neural network of  $L$  layers. For each layer  $l$  parameterized with  $\theta_l$ , the operation of a feedforward neural network can be described as

$$\mathbf{x}_{l+1} = f_{\theta_l}(\mathbf{x}_l), \quad (1)$$

where  $\mathbf{x}_l \in \mathbb{R}^d$  represents the output from the preceding layer, and  $f_{\theta_l}$  denotes the transformation applied at the current layer. Although it possesses a notable capability for feature abstraction, it is widely recognized that in the context of building deeper models, pure feedforward architectures are prone to vanishing gradients.

**Residual connections.** To address the optimization problem of vanishing gradients in deeper neural networks, ResNets [24] constructs each layer as a residual function, resulting in a modification to Eq. 1:

$$\mathbf{x}_{l+1} = \mathbf{x}_l + f_{\theta_l}(\mathbf{x}_l). \quad (2)$$

This design builds shortcuts from input to output, allowing gradient magnitude to be preserved regardless of the depth of the model. However, a consequence of this design is that the output stays close to the input in practice [22], defeating the need to construct complex transformations over depth. The same phenomenon is also observed in highway networks [59], which adopt learnable gates  $H_\phi(\mathbf{x}) \in [0, 1]^d$  in both the residual and skip branches:  $\mathbf{x}_{l+1} =$

$H_\phi(\mathbf{x}_l) \cdot \mathbf{x}_l + (1 - H_\phi(\mathbf{x}_l)) \cdot f_{\theta_l}(\mathbf{x}_l)$ . Although this flexible design allows the model to build the abstraction level over depths, similar to feedforward networks, Srivastava et al. [60] finds  $H_\phi \approx 1$  for most units, suggesting the model prefers copying the input.

### Decayed identity shortcuts for unsupervised representation learning.

Setting aside the optimization benefits brought by residual connections, we rethink the role of the residual connections from the viewpoint of representation learning. Abstraction can be viewed as invariance to local changes of input and is crucial to the disentanglement of the feature space [7]. Prior work suggests that a shortcut path of residual connections tends to preserve high-frequency fine-grained information of input [22] resulting in decreased feature abstraction. We hypothesize that this lack of abstraction harms the capability of the model to learn meaningful low-level features and that ensuring an abstract structure in the deeper layers of the neural network will help improve representation learning, especially for unsupervised tasks that often use indirect proxy objectives, such as pixel-wise reconstruction loss. Motivated by this hypothesis, we propose to downweight the contribution from the shortcut path:

$$\mathbf{x}_{l+1} = \alpha_l \mathbf{x}_l + f_{\theta_l}(\mathbf{x}_l), \quad (3)$$

where  $\alpha_l \in [0, 1]$  is a rescaling factor to the residual path, controlling the information flow through the skip connection. Fully expanding this relation for a network with  $L$  layers indexed from 0 to  $L - 1$ , we have that

$$\mathbf{x}_L = \left( \prod_{l=0}^{L-1} \alpha_l \right) \mathbf{x}_0 + \sum_{l=0}^{L-2} \left( \prod_{i=l+1}^{L-1} \alpha_i \right) f_{\theta_l}(\mathbf{x}_l) + f_{\theta_{L-1}}(\mathbf{x}_{L-1}). \quad (4)$$

We see that the contribution of the input  $\mathbf{x}_0$  is scaled by each  $\alpha_l \leq 1$  while each subsequent network block output  $f_{\theta_l}(\mathbf{x}_l)$  omits scaling factors up to  $\alpha_l$ . Hence, the contribution of early features of the network is especially down-weighted, preventing the network from passing fine-grained detailed information to the bottleneck  $X_L$ .

**Decay schema.** Rather than adopting a naive choice of  $\alpha_l$  as a constant across all layers, we choose  $\alpha_l$  to be a function parameterized by the layer index  $l$ , where the contribution from the shortcut path is monotonically decreasing when  $l$  increases:

$$\alpha_l = 1 - \delta_\alpha l, \quad (5)$$

where  $\delta_\alpha := \frac{(1 - \alpha_{\min})}{L}$ ,  $\alpha_{L-1} \equiv \alpha_{\min}$  is a minimum scaling factor applied at the final layer  $L - 1$ . Our formulation brings two primary benefits. First,  $\alpha_l$ , as a linear interpolation between 0 and 1, acts as a smooth transition between residual connections and feedforward layers, bringing us the optimization benefits seen in the residual connections, while simultaneously encouraging learning the deeper layers to learn more abstract representations. Second, similar to the naive formulation, our method only introduces one extra hyperparameter  $\alpha_{\min}$ , which is not data-dependent and does not need to be learned.

### 3.2 Implementation Strategy

**Skip connections for Autoencoders.** Since our method progressively decays the residual connections over network depth, it encourages the most abstract features to be learned by the final layer. Hence, when using our strategy on an Autoencoder architecture, we only apply residual decay to the encoder layers. However, learning a highly abstract bottleneck is detrimental to the training objectives that aim for pixel-wise reconstruction, as they necessitate the preservation of information at the bottleneck across all feature levels. To address this, we incorporate standard skip connections between the encoder and decoder, enabling the encoder to directly pass information from shallow layers to the decoder while learning increasingly abstract representations in the deeper encoder layers.

**Stabilizing training with residual zero initialization.** The model exhibits rapid feature norm growth at the beginning of training for  $\alpha_{\min} \leq 0.7$ . We suspect that the model learns to amplify the output feature norm of  $f_{\theta_i}(\mathbf{x})$  to counteract the significant decay applied to the residual connection. This growth leads to training instability and negatively impacts training convergence. To address this issue, we follow previous works [27] and initialize the weights of the final output layer in each  $f_{\theta_i}$  to zero instead of using the original Xavier uniform initialization [20]. This approach significantly enhances training stability by limiting the rate of feature norm growth and enables us to explore training with even lower values of  $\alpha_{\min}$ .

## 4 Large-scale Experiments

**Masked Autoencoders.** We implement our method within a Masked Autoencoder (MAE) [26] by replacing the residual connections in the encoder’s MLP and attention blocks with decayed identity shortcuts. The MAE operates by accepting images with a random subset of pixels masked out and learning to recover the discarded pixels. As Section 3.2 describes, we add skip connections between the encoder and decoder to facilitate learning abstract representations at the bottleneck. Since the original MAE has twice the number of encoder layers as decoder layers, we inject output from every other encoder layer into the corresponding decoder layer. To match spatial dimensions, injected encoder features are combined with learnable masked tokens before channel-wise concatenation.

**Experimental setup.** To evaluate the learned features, we first pre-train the MAE on the ImageNet-1K dataset [15] and then conduct linear probing on a learned class token from pre-trained features over the test set using a single linear layer. We also conduct ablations on ImageNet-100. For fair comparison, our baseline methods are (1) the original MAE as well as (2) our framework with  $\alpha_{\min} = 1$ , which is equivalent to an MAE with skip connections. For MAE hyperparameters, including the learning rate schedule, total training epochs, and mask ratio, we follow the best settings found in the original paper. Please see the appendix in supplementary materials for detailed experimental setups.

Method	Backbone	Objective	Augmentation	Accuracy
MoCo-v2[11]	ResNet-50	Contrastive Loss	Full	71.1
MoCo-v3[12]	VIT-B/16	Contrastive Loss	Full	76.7
SimCLR-v2[10]	ResNet-50	Contrastive Loss	Full	77.7
DINO[8]	VIT-B/16	Contrastive Loss	Full	78.2
iBOT[65]	VIT-B/16	Contrastive Loss	Full+Mask	<b>79.5</b>
Data2Vec[4]	VIT-B/16	Feature Loss	Full+Mask	68.0
CAE[13]	VIT-B/16	Recon. + Feature Loss	Affine+Mask	70.4
I-JEPA[3]	VIT-B/16	Feature Loss	Affine+Mask	<b>72.9</b>
MAE[26]	VIT-B/16	Recon. Loss	Affine+Mask	67.3*
Ours ( $\alpha_{\min} = 0.6$ )	VIT-B/16	Recon. Loss	Affine+Mask	<b>72.3</b>

**Table 1: Accuracy of linear classifier based on pre-trained learned representations on the ImageNet-1K dataset.** We list the training objective and data augmentation process of each method. Training objectives include contrastive losses, feature losses, and image reconstruction. Affine data augmentation represents random flip, random crop, and resize. Full augmentation combines affine augmentation and color distortion. With our simple modification, we substantially improve the MAE baseline by encouraging the model to learn an increased abstract features over depth. We achieve competitive performance compared to I-JEPA which uses an explicit feature loss. \*We report the results using our evaluation script, while the official MAE script gives 67.8%.

## 4.1 ImageNet-1K

We evaluate our learned representation using the ImageNet-1k dataset [15] and report the results in Table 1 by training a linear classifier on top of frozen backbone features. In the table, we show the linear probing performance of various self-supervised methods, which we categorize by their architecture, objectives, and data augmentation processes. In the top half of the table, we present methods that employ a contrastive loss. Although these methods produce the best probing accuracies, their success depends on a carefully designed data augmentation process, which may need to be tuned for each different data distribution. In the bottom half, we show several methods, including ours, which do not rely on contrastive objectives. With the exception of Data2Vec, these methods only use a standard random affine data transformation (with random masking), which need not be distribution-reliant. Among these methods, MAE only uses a pixel-wise loss, I-JEPA and CAE use a latent feature alignment loss, and CAE uses both. Our method simply extends MAE by constructing an implicit feature bottleneck and shows significant improvements over the MAE baselines (72.3% *vs.* 67.3%), outperforming Data2Vec and CAE and giving a probing accuracy competitive with I-JEPA, without needing to use explicit feature alignment.

## 4.2 Qualitative Experiments.

We qualitatively evaluate the capability of our method to reconstruct test images and learn semantic image embeddings on ImageNet-100.



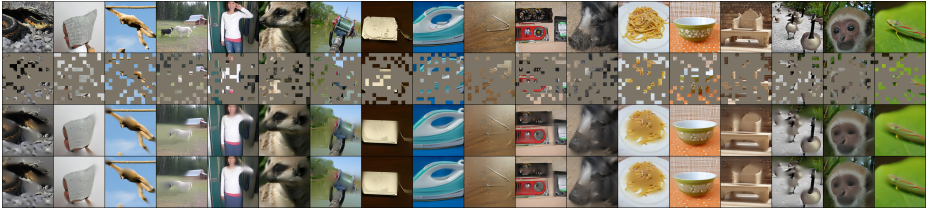


**Fig. 2: Qualitative comparison of images reconstructed by MAE with and without our method.** We observe our method learns features with higher linear probing accuracy without compromising reconstruction quality. Row 1: ground truth test image. Row 2: images masked at 75%. Row 3: reconstructions with our method. Row 4: reconstructions with baseline MAE.

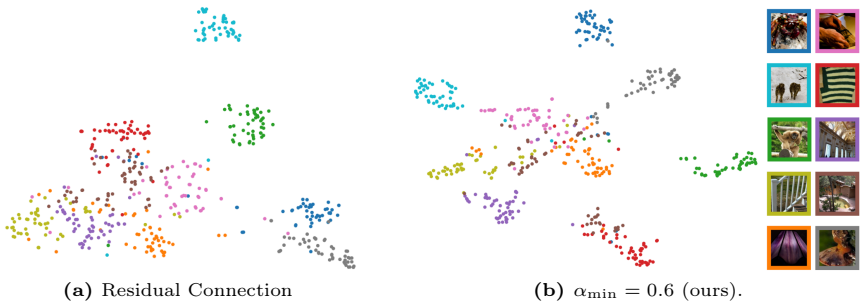


**Fig. 3: Comparison of t-SNE visualization for models trained with (a) standard Residual Connection and (b) our method with  $\alpha_{\min} = 0.6$ .** We use the models trained in Section 4.3 on ImageNet-100 to produce features for *test samples*. The visualization of t-SNE embeddings is performed on a subset comprising 10 classes selected at random. Representative images for each category along with their plot color are given on the right. We observe that the embeddings of some categories for the model trained with standard residual connections (a) have collapsed together while our method (b) forms well structured clusters.

**Reconstruction.** We qualitatively evaluate test images reconstructed by an MAE using our framework and images reconstructed by the original MAE. We show the reconstructed images in Figure 2. While the focus of our work is entirely to improve the representations learned by an encoder, we observe that our framework does not harm the reconstructions. Hence, there is no qualitative tradeoff for our increase in linear probing accuracy.

**Embedding visualization.** We also qualitatively evaluate the feature learning in Figure 3 by visualizing the t-SNE embeddings of the learned features for a random subset of test images. While the Residual connection (baseline) embeddings in Figure 3a produce some separation, they struggle to differentiate some harder categories, such as tubs (brown), stairs (yellow), and church buildings (purple). In contrast, the embeddings produced from our features in Figure 3b

<b>Backbone</b> \ $\alpha_{\min}$	0.5	0.6	0.7	0.8	0.9	1.0
ViT-B/16	82.3	<b>83.6</b>	81.8	79.8	79.2	76.5
ViT-S/16	<b>78.6</b>	78.5	78.1	75.2	73.5	69.2

**Table 2: Linear Probing Accuracy on ImageNet-100 for our method varying  $\alpha_{\min}$  and architecture size.** We conduct ablation studies and demonstrate that linear probing performance for both architectures increases as  $\alpha_{\min}$  decreases until around 0.5-0.6. While the larger ViT-B/16 architecture achieves the highest accuracy of 83.6, it is noteworthy that the smaller ViT-S/16, when utilizing our method, outperforms the baseline setting (standard Residual Connection at  $\alpha_{\min} = 1$ ) of ViT-B/16 MAE.

display much clearer separation and are able to separate almost all categories distinctly.

### 4.3 Ablation

We conduct ablations on several properties of our framework on ImageNet-100. A summary of results can be found in Tables 2 and 3.

**Maximum decay rate.** The only parameter of our framework is  $\alpha_{\min}$ , the maximum rate of decay of the identity shortcut in a residual connection. In Table 2, we show linear probing scores for varying values of  $\alpha_{\min}$ . We observe that  $\alpha_{\min}$  must be sufficiently small to regularize the flow of information through the residual connection effectively. A reasonably small  $\alpha_{\min}$  prevents the deeper layers of the encoder from relying heavily on the residual connections, allowing for more abstract representations in the bottleneck. This yields up to a 7.1% improvement over the ViT-B/16 baseline ( $\alpha_{\min} = 1$ ) in linear probing accuracy on ImageNet-100. On the other hand, if  $\alpha_{\min}$  is too small, for example,  $\alpha_{\min} \leq 0.4$  for ViT-B/16, we observe that the training becomes unstable.

**Architecture size.** In Table 2, we also train both the ViT-B/16 and the smaller ViT-S/16 backbone using varying  $\alpha_{\min}$ . Our framework is especially effective on the smaller architecture, increasing linear probing performance by 9.4%, compared to the baseline setting (standard Residual Connection at  $\alpha_{\min} = 1$ ). This is consistent with the observation that larger models generalize better [31] than smaller models. Our method is able to significantly improve the smaller ViT-S/16 and slightly close the gap between the differently-sized architectures.

**Skip connections.** Another critical design choice in our network is to include skip connections that are not in the original MAE. As discussed in Section 3.2, if the MAE does not use skip connections that give the network a shortcut to pass low-level detail information from the encoder to the decoder, the bottleneck layer must preserve enough information to reconstruct the input image accurately. This is opposed to the design of the shortcut decay, which prompts the bottleneck to learn abstract representations. These contrary effects significantly degrade the representation learned by the model, leading to a 22.1% drop in the linear probing score, as we report in Table 3a.

Configurations	UNet	Accuracy
$\alpha_{\min} = 0.6$	No	61.5
$\alpha_{\min} = 0.6$	Yes	<b>83.6*</b>

(a) **Effect of Skip Connections.** Applying the framework without skip connections designed in Section 3.2 results in a severe drop in representation quality.

Configurations	Decay Block	$\alpha_{\min}$	Accuracy
$\mathbf{x}_{l+1} = \mathbf{x}_l + \sqrt{0.5}f_{\theta_l}(\mathbf{x}_l)$	MLP & Atten.	–	76.9
$\mathbf{x}_{l+1} = \sqrt{0.5}(\mathbf{x}_l + f_{\theta_l}(\mathbf{x}_l))$	MLP & Atten.	–	82.6
$\mathbf{x}_l = \alpha_l \mathbf{x}_l + f_{\theta}(\mathbf{x}_l)$	Atten.	0.6	79.3
$\mathbf{x}_l = \alpha_l \mathbf{x}_l + f_{\theta}(\mathbf{x}_l)$	MLP	0.6	80.6
$\mathbf{x}_l = \alpha_l \mathbf{x}_l + f_{\theta}(\mathbf{x}_l)$	MLP & Atten.	0.6	<b>83.6*</b>

(b) **Other Decay Schemas.** We conduct ablations using a variety of scalings of the residual connection. We observe that our full method produces the best results.

**Table 3: Linear probing accuracy of ablation experiments using ViT-B/16 on ImageNet-100.** \*We duplicate the performance of our  $\alpha_{\min} = 0.6$  result from Table 2 for comparison.

**Different decay schema.** In Section 3.1, we define our shortcut decay as a decreasing weight over every residual connection in the encoder. In Table 3b, we apply our framework to different network components within the encoder. Specifically, we test restricting shortcut decay to only attention blocks and only MLP blocks within each transformer block. While our framework does work well and gives similar results in these settings, we do observe a performance drop using the same  $\alpha_{\min}$ . This can be explained by the reduction in the number of weighted connections. By halving the number of weighted residuals, an increase in the decay rate is required to match the quality of learned representations. Hence, our framework is actually robust against particular design choices of *which* connections are decayed but relies more on the *total* rate of information decay throughout the encoder.

We also explore a different parameterization of the residual connection. A few existing works leverage the benefits of re-scaling the residual connections in the context of image generation tasks [34, 35, 37, 57], but all of them scale *both* branches of the residual block *jointly*. Following this design, we try applying a constant factor  $\alpha = \sqrt{0.5}$  to *both*  $\mathbf{x}$  and  $f_{\theta_l}(\mathbf{x})$ , as seen in the implementation of Karras et al. [37]. In Table 3b, we observe that including such constant re-scaling to both branches decreases the linear probing score of the model. We also try applying a constant scaling factor to only  $f_{\theta_l}(\mathbf{x})$ , a case studied by [18]. These two ablations confirm that the key to abstract representation learning is controlling the weight of the identity shortcut path, leveraging the structural bias reminiscent of feedforward neural networks.

## 5 Discussion

In this section, we try to answer a key question: How and why do residual connections impact the abstraction level of the deeper layers in a neural network? We delve deeper into how our design reinforces the low-rank bias of neural networks and try to connect our method to ideas in existing works [31]. To this end, we visualize the training dynamics of our method in both the supervised and unsupervised settings to provide a holistic analysis.

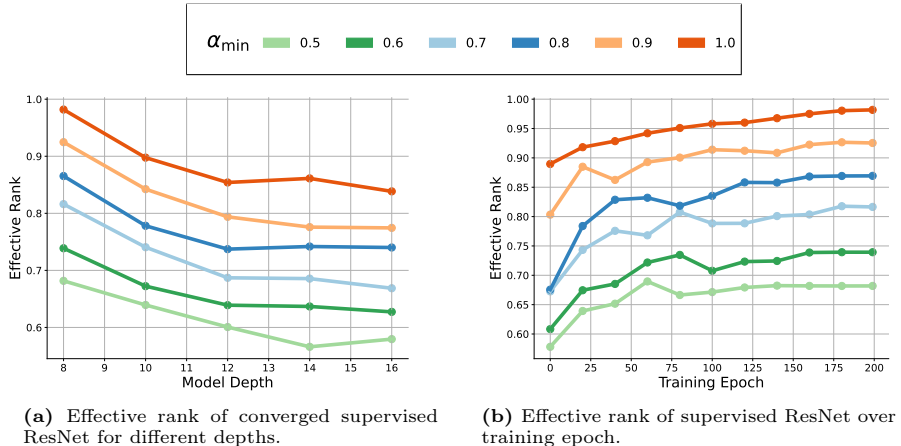


**Fig. 4:** We train ResNet models for classification on a small subset of ImageNet and visualize (a) effective rank across different depths at convergence and (b) training dynamics of effective rank over time for various  $\alpha_{\min}$ . In (a) we see that at convergence, our method consistently decreases the feature rank with various depth and, in (b), this pattern is also shown for standard ResNet model at every stage of training.

**Low-rank simplicity bias.** Huh et al. [31] investigate the low-rank simplicity bias in deeper feed-forward neural networks, which drives neural networks to find low-rank solutions. At the same time, they make an empirical observation that deeper residual networks do not show a similar rank contracting behavior.

**Effective rank.** To quantify the rank of the learned representation, Huh et al. [31] use *effective rank*, which is a continuous measure. For a matrix  $\mathbf{A} \in \mathbb{R}^{m \times n}$ , the effective rank  $\rho(\mathbf{A})$  is defined as the Shannon entropy of the normalized singular values [51]:

$$\rho(\mathbf{A}) = - \sum_i^{\min(n,m)} \bar{\sigma}_i \log \bar{\sigma}_i, \quad (6)$$

where  $\bar{\sigma}_i = \sigma_i / \sum_j \sigma_j$  denotes the  $i^{\text{th}}$  normalized singular value. Intuitively, this measure is small when a few singular values dominate and large when singular values are evenly spread, hence giving a good continuous approximation for matrix rank.

In the following subsections, to compute the effective rank, we use the singular values from the covariance matrix  $\mathbf{A}_{\theta}$  of the last-layer features, where  $\mathbf{A}_{\theta}(i, j)$  denotes the covariance of the learned class tokens for the  $i^{\text{th}}$  and  $j^{\text{th}}$  samples.

## 5.1 Abstraction and Low-rank in the Supervised Setting

Inspired by their analysis, *we conjecture that the improvement to feature learning capability of our method can mainly be attributed to the decayed identity shortcuts promoting low-rank features at the bottleneck.* To verify our conjecture

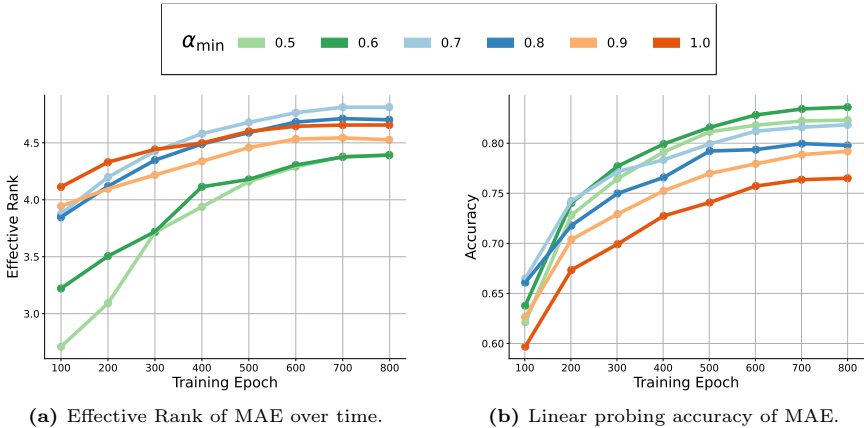


**Fig. 5:** We visualize (a) the training dynamics of effective rank for various  $\alpha_{\min}$  and (b) the linear probing accuracy for various  $\alpha_{\min}$  for unsupervised Masked Autoencoders (MAE) trained on ImageNet-100. These features are extracted from the bottleneck layer of the MAE encoder. In (a) we observe that  $\alpha_{\min} = 0.6$  and  $\alpha_{\min} = 0.5$  produce features with the lowest effective rank. In (b) we observe that accuracy improves with lower  $\alpha_{\min}$ .

and evaluate how our method affects the effective rank of the output feature matrices, we apply our method to a supervised classification task on a 10-class subset of ImageNet, ensuring that our model is over-parameterized, following the experimental setup in [31].

We first follow the evaluation setup in [31] to analyze the impact of the model depth on feature rank when applying our method. In this experiment, we modify the standard ResNet-18 model to experiment with different depth models. By default, the ResNet-18 has a total of 8 residual blocks that are equally distributed into 4 layers. To increase model depth, we repeat residual blocks in the 3rd layer to obtain models varying between 8 and 16 total layers. At convergence, we observe that the models of different depths achieve a similar test accuracy. However, despite similar accuracies, in Figure 4a, which visualizes the effective rank over depth for different values of  $\alpha_{\min}$ , we see that the effective rank decreases over depth. Furthermore, smaller values of  $\alpha_{\min}$  consistently lead to features with lower effective rank.

Next, in Figure 4b, we try to verify our conjecture by visualizing the evolution of effective rank during training when choosing different  $\alpha_{\min}$  in our method. For this experiment, we choose to train the standard ResNet-18 using our decayed identity shortcuts. In this setup, we observe that the optimal choice of  $\alpha_{\min}$  slightly improves the test accuracy of the classification network: 94.4% with  $\alpha_{\min} = 0.7$  vs. 93.6% with  $\alpha_{\min} = 1.0$ . We observe that the effective rank of the final features decreases with decreasing  $\alpha_{\min}$ . This supports our hypothesis that (1) decayed identity shortcuts substantially decrease the rank of bottleneck features and (2) decreasing feature rank may help improve learned features.

## 5.2 Abstraction and Low-rank in the Unsupervised Setting

We would like to verify if our previous observations in supervised tasks hold for unsupervised feature learning. Specifically, we measure the training dynamics of the models trained in Table 2 (MAEs trained on ImageNet-100) in terms of accuracy and the effective rank. In Figures 5a and 5b, we visualize the effective rank and linear probing accuracy of these models throughout training.

In Figure 5a, we show that in the first 300 epochs of training, our framework can substantially decrease the effective rank of  $\rho(\mathbf{A}_\theta)$ . At this stage, from Figure 5b, we can see that our model with  $\alpha_{\min} = 0.6$  achieves a maximal improvement of 7.8% over the baseline with  $\alpha_{\min} = 1.0$ . As training continues, models with lower  $\alpha_{\min}$  consistently achieve higher probing scores. However, while the  $\alpha_{\min} = 0.5$  and 0.6 models have the lowest effective feature ranks, supporting the conjecture that low-rank features lead to better abstractions, we do observe outliers in  $\alpha_{\min} = 0.7$  and 0.8 having larger feature ranks.

Overall, along with the empirical observations found in Section 5.1 in the supervised scenario, we have uncovered evidence supporting our conjecture that *an appropriate low-rank bias helps abstract representation learning* and shortcut decay in residual connections promotes this bias, enhancing representation learning performance.

## 6 Conclusion

Huh et al. [31] raise a key insight in their work – that how a neural network is parameterized matters for fitting the data – and investigate the inductive low-rank bias of stacking more linear layers in a network.

In this work, we observe that the ubiquitous residual network [24] may not be the ideal network parametrization for representation learning and propose a modification of the shortcut path in residual blocks that significantly improves unsupervised representation learning. We explore the connection between our reparameterization of the residual connection and the effective rank of the learned features, finding a correlation between good representations and low-rank representations.

Our work calls into question a fundamental design choice of neural networks that has been used in many modern architectures. By rethinking this choice, the door is open for further reparametrizations and improvements to unsupervised representation learning. The results we show provide a prompt for more extensive investigations into the connection between low effective rank and high-quality abstract representations, as well as the exploration of underlying theoretical mechanisms for this relationship.

## 7 Acknowledgement

RJ and RW gratefully acknowledge the support of AFOSR grants FA9550-18-1-0166, NSF grants DMS-2023109, and NSF grants PHY2317138.

# Bibliography

- [1] J. Achiam, S. Adler, S. Agarwal, L. Ahmad, I. Akkaya, F. L. Aleman, D. Almeida, J. Altenschmidt, S. Altman, S. Anadkat, et al. Gpt-4 technical report. *arXiv:2303.08774*, 2023.
- [2] S. Arora, N. Cohen, W. Hu, and Y. Luo. Implicit regularization in deep matrix factorization. *NeurIPS*, 2019.
- [3] M. Assran, Q. Duval, I. Misra, P. Bojanowski, P. Vincent, M. Rabbat, Y. LeCun, and N. Ballas. Self-supervised learning from images with a joint-embedding predictive architecture. In *CVPR*, 2023.
- [4] A. Baevski, W.-N. Hsu, Q. Xu, A. Babu, J. Gu, and M. Auli. Data2vec: A general framework for self-supervised learning in speech, vision and language. In *ICML*, 2022.
- [5] H. Bao, L. Dong, S. Piao, and F. Wei. Beit: Bert pre-training of image transformers. *arXiv:2106.08254*, 2021.
- [6] D. Beaglehole, A. Radhakrishnan, P. Pandit, and M. Belkin. Mechanism of feature learning in convolutional neural networks. *arXiv:2309.00570*, 2023.
- [7] Y. Bengio, A. Courville, and P. Vincent. Representation learning: A review and new perspectives. *TPAMI*, 2013.
- [8] M. Caron, H. Touvron, I. Misra, H. Jégou, J. Mairal, P. Bojanowski, and A. Joulin. Emerging properties in self-supervised vision transformers. In *ICCV*, 2021.
- [9] T. Chen, S. Kornblith, M. Norouzi, and G. Hinton. A simple framework for contrastive learning of visual representations. In *ICML*, 2020.
- [10] T. Chen, S. Kornblith, K. Swersky, M. Norouzi, and G. E. Hinton. Big self-supervised models are strong semi-supervised learners. *NeurIPS*, 2020.
- [11] X. Chen, H. Fan, R. Girshick, and K. He. Improved baselines with momentum contrastive learning. *arXiv:2003.04297*, 2020.
- [12] X. Chen, S. Xie, and K. He. An empirical study of training self-supervised vision transformers. In *ICCV*, 2021.
- [13] X. Chen, M. Ding, X. Wang, Y. Xin, S. Mo, Y. Wang, S. Han, P. Luo, G. Zeng, and J. Wang. Context autoencoder for self-supervised representation learning. *IJCV*, 2024.
- [14] Y. Cheng. Mean shift, mode seeking, and clustering. *TPAMI*, 1995.
- [15] J. Deng, W. Dong, R. Socher, L.-J. Li, K. Li, and L. Fei-Fei. Imagenet: A large-scale hierarchical image database. In *CVPR*, 2009.
- [16] Y. Dong, J.-B. Cordonnier, and A. Loukas. Attention is not all you need: Pure attention loses rank doubly exponentially with depth. In *ICML*, 2021.
- [17] A. Dosovitskiy, L. Beyer, A. Kolesnikov, D. Weissenborn, X. Zhai, T. Unterthiner, M. Dehghani, M. Minderer, G. Heigold, S. Gelly, et al. An image is worth 16x16 words: Transformers for image recognition at scale. *arXiv:2010.11929*, 2020.
- [18] K. Fischer, D. Dahmen, and M. Helias. Optimal signal propagation in ResNets through residual scaling. *arXiv:2305.07715*, 2023.

- [19] B. Geshkovski, C. Letrouit, Y. Polyanskiy, and P. Rigollet. The emergence of clusters in self-attention dynamics. *NeurIPS*, 2024.
- [20] X. Glorot and Y. Bengio. Understanding the difficulty of training deep feedforward neural networks. In *ICAIIS*, 2010.
- [21] I. Goodfellow, J. Pouget-Abadie, M. Mirza, B. Xu, D. Warde-Farley, S. Ozair, A. Courville, and Y. Bengio. Generative adversarial nets. *NeurIPS*, 2014.
- [22] K. Greff, R. K. Srivastava, and J. Schmidhuber. Highway and residual networks learn unrolled iterative estimation. *arXiv:1612.07771*, 2016.
- [23] J.-B. Grill, F. Strub, F. Althché, C. Tallec, P. Richemond, E. Buchatskaya, C. Doersch, B. Avila Pires, Z. Guo, M. Gheshlaghi Azar, et al. Bootstrap your own latent—a new approach to self-supervised learning. *NeurIPS*, 2020.
- [24] K. He, X. Zhang, S. Ren, and J. Sun. Deep residual learning for image recognition. In *CVPR*, 2016.
- [25] K. He, H. Fan, Y. Wu, S. Xie, and R. Girshick. Momentum contrast for unsupervised visual representation learning. In *CVPR*, 2020.
- [26] K. He, X. Chen, S. Xie, Y. Li, P. Dollár, and R. Girshick. Masked autoencoders are scalable vision learners. In *CVPR*, 2022.
- [27] J. Ho, A. Jain, and P. Abbeel. Denoising diffusion probabilistic models. *NeurIPS*, 2020.
- [28] S. Hochreiter and J. Schmidhuber. Long short-term memory. *Neural computation*, 1997.
- [29] G. Huang, Z. Liu, L. Van Der Maaten, and K. Q. Weinberger. Densely connected convolutional networks. In *CVPR*, 2017.
- [30] Z. Huang, X. Jin, C. Lu, Q. Hou, M.-M. Cheng, D. Fu, X. Shen, and J. Feng. Contrastive masked autoencoders are stronger vision learners. *TPAMI*, 2023.
- [31] M. Huh, H. Mobahi, R. Zhang, B. Cheung, P. Agrawal, and P. Isola. The low-rank simplicity bias in deep networks. *arXiv:2103.10427*, 2021.
- [32] S. Ioffe and C. Szegedy. Batch normalization: Accelerating deep network training by reducing internal covariate shift. In *ICML*, 2015.
- [33] L. Jing, J. Zbontar, et al. Implicit rank-minimizing autoencoder. *NeurIPS*, 2020.
- [34] T. Karras, T. Aila, S. Laine, and J. Lehtinen. Progressive growing of gans for improved quality, stability, and variation. *arXiv:1710.10196*, 2017.
- [35] T. Karras, S. Laine, M. Aittala, J. Hellsten, J. Lehtinen, and T. Aila. Analyzing and improving the image quality of stylegan. In *CVPR*, 2020.
- [36] T. Karras, S. Laine, and T. Aila. A style-based generator architecture for generative adversarial networks. *TPAMI*, 2021.
- [37] T. Karras, M. Aittala, T. Aila, and S. Laine. Elucidating the design space of diffusion-based generative models. *NeurIPS*, 2022.
- [38] D. P. Kingma and M. Welling. Auto-encoding variational bayes. *arXiv:1312.6114*, 2013.
- [39] A. Kirillov, E. Mintun, N. Ravi, H. Mao, C. Rolland, L. Gustafson, T. Xiao, S. Whitehead, A. C. Berg, W.-Y. Lo, et al. Segment anything. *arXiv:2304.02643*, 2023.



- [40] T. Kojima, S. S. Gu, M. Reid, Y. Matsuo, and Y. Iwasawa. Large language models are zero-shot reasoners. *NeurIPS*, 2022.
- [41] G. Larsson, M. Maire, and G. Shakhnarovich. FractalNet: Ultra-deep neural networks without residuals. *ICLR*, 2017.
- [42] M. T. R. Laskar, M. S. Bari, M. Rahman, M. A. H. Bhuiyan, S. Joty, and J. X. Huang. A systematic study and comprehensive evaluation of chatgpt on benchmark datasets. *arXiv:2305.18486*, 2023.
- [43] T. Li, H. Chang, S. Mishra, H. Zhang, D. Katabi, and D. Krishnan. Mage: Masked generative encoder to unify representation learning and image synthesis. In *CVPR*, 2023.
- [44] I. Loshchilov and F. Hutter. Decoupled weight decay regularization. *arXiv:1711.05101*, 2017.
- [45] B. Neyshabur, Z. Li, S. Bhojanapalli, Y. LeCun, and N. Srebro. Towards understanding the role of over-parametrization in generalization of neural networks. *arXiv:1805.12076*, 2018.
- [46] A. Radhakrishnan, D. Beaglehole, P. Pandit, and M. Belkin. Feature learning in neural networks and kernel machines that recursively learn features. *arXiv:2212.13881*, 2022.
- [47] A. Radhakrishnan, M. Belkin, and D. Drusvyatskiy. Linear recursive feature machines provably recover low-rank matrices. *arXiv:2401.04553*, 2024.
- [48] A. Ramesh, M. Pavlov, G. Goh, S. Gray, C. Voss, A. Radford, M. Chen, and I. Sutskever. Zero-shot text-to-image generation. In *ICML*, 2021.
- [49] R. Rombach, A. Blattmann, D. Lorenz, P. Esser, and B. Ommer. High-resolution image synthesis with latent diffusion models. In *CVPR*, 2022.
- [50] O. Ronneberger, P. Fischer, and T. Brox. U-Net: Convolutional networks for biomedical image segmentation. In *MICCAI*, 2015.
- [51] O. Roy and M. Vetterli. The effective rank: A measure of effective dimensionality. In *ESPC*, 2007.
- [52] P. Savarese and D. Figueiredo. Residual gates: A simple mechanism for improved network optimization. In *ICLR*, 2017.
- [53] C. Schuhmann, R. Beaumont, R. Vencu, C. Gordon, R. Wightman, M. Cherti, T. Coombes, A. Katta, C. Mullis, M. Wortsman, et al. Laion-5b: An open large-scale dataset for training next generation image-text models. *NeurIPS*, 2022.
- [54] Z. Shi, X. Zhou, X. Qiu, and X. Zhu. Improving image captioning with better use of captions. *arXiv:2006.11807*, 2020.
- [55] M. Singh, Q. Duval, K. V. Alwala, H. Fan, V. Aggarwal, A. Adcock, A. Joulin, P. Dollár, C. Feichtenhofer, R. Girshick, et al. The effectiveness of mae pre-pretraining for billion-scale pretraining. *arXiv:2303.13496*, 2023.
- [56] J. Song, C. Meng, and S. Ermon. Denoising diffusion implicit models. *ICLR*, 2021.
- [57] Y. Song, J. Sohl-Dickstein, D. P. Kingma, A. Kumar, S. Ermon, and B. Poole. Score-based generative modeling through stochastic differential equations. *arXiv:2011.13456*, 2020.

- [58] Y. Song, P. Dhariwal, M. Chen, and I. Sutskever. Consistency models. *arXiv:2303.01469*, 2023.
- [59] R. K. Srivastava, K. Greff, and J. Schmidhuber. Highway networks. *arXiv:1505.00387*, 2015.
- [60] R. K. Srivastava, K. Greff, and J. Schmidhuber. Training very deep networks. *NeurIPS*, 2015.
- [61] C. Szegedy, W. Liu, Y. Jia, P. Sermanet, S. Reed, D. Anguelov, D. Erhan, V. Vanhoucke, and A. Rabinovich. Going deeper with convolutions. In *CVPR*, 2015.
- [62] G. Team, R. Anil, S. Borgeaud, Y. Wu, J.-B. Alayrac, J. Yu, R. Soricut, J. Schalkwyk, A. M. Dai, A. Hauth, et al. Gemini: a family of highly capable multimodal models. *arXiv:2312.11805*, 2023.
- [63] A. Vaswani, N. Shazeer, N. Parmar, J. Uszkoreit, L. Jones, A. N. Gomez, Ł. Kaiser, and I. Polosukhin. Attention is all you need. *NeurIPS*, 2017.
- [64] Z. Wu, Y. Xiong, S. X. Yu, and D. Lin. Unsupervised feature learning via non-parametric instance discrimination. In *CVPR*, 2018.
- [65] J. Zhou, C. Wei, H. Wang, W. Shen, C. Xie, A. Yuille, and T. Kong. ibot: Image bert pre-training with online tokenizer. *arXiv:2111.07832*, 2021.
- [66] L. Zhu, R. Deng, M. Maire, Z. Deng, G. Mori, and P. Tan. Sparsely aggregated convolutional networks. In *ECCV*, 2018.
- [67] L. Zhu, R. Deng, M. Maire, Z. Deng, G. Mori, and P. Tan. Sparsely aggregated convolutional networks. In *ECCV*, 2018.

## 8 Appendix

### 8.1 Training and Evaluation Details of Masked Autoencoders

**Model training.** Our training configurations primarily followed the guidelines established by He et al. [26]. In the ImageNet-1K experiment, our model was trained for 800 epochs, utilizing the AdamW [44] optimizer with a constant weight decay of  $5e-2$  for a batch size of 1024. We set the maximum learning rate to  $6e-4$ . Initially, the learning rate started at 0 and linearly increased to its maximum over the first 40 epochs, after which it followed a cosine schedule to gradually decrease to zero by the end of the training period. It is worth noting that the learning rate per sample, or effective learning rate, in our setup matched that of He et al. [26], although our maximum learning rate was set lower due to our batch size being a quarter of theirs. We applied random resizing, cropping, and horizontal flipping during training as part of our augmentation scheme. To enhance the quality of the learned representations in most experiments, we employed the normalized pixel loss, as proposed by [26]. For visualization purposes, as shown in Figure 2, we used L2 pixel-wise loss. In the ImageNet-100 experiment, we employed the identical training configuration used in the ImageNet-1K experiments.

**Evaluation with Linear Probing.** We found the evaluation protocols from He et al. [26] were less optimal for our model and led to a long training time for the linear classifier on the ImageNet-1K dataset. Their reported training time on linear probing is 75 GPU hours using V100 GPUs, which we found to be mainly due to their need for on-the-fly random data augmentation at each epoch. To address this, we implemented alternative evaluation configurations: For the training of the linear classifier, instead of employing random data augmentation at every epoch, we opted to precompute the features for each image using three variations of random data augmentations and one instance of central cropping. This produced four sets of precomputed features per image. During each training epoch, we then randomly selected one set of these precomputed features. The linear classifier was updated using the AdamW [44] optimizer over 200 epochs. The learning rate was set to linearly warm up to  $1e-2$  during the initial 20 epochs, followed by a decay to zero towards the end using a cosine scheduler. This process utilized a batch size of 5120 across 4 GPUs. Employing precomputed features significantly reduced our total training time from 75 V100 GPU hours to 2.7 GPU hours on A6000 GPUs. As a result, we observed a slight decrease in the Top-1 linear probing accuracy of the ViT-B/16 model, from 67.8% as reported by [26], to 67.3% with our revised evaluation setup.

For the ImageNet-100 dataset, we employed a simpler evaluation protocol: We train the linear classifier with a batch size of 1024 for 200 epochs, where the learning rate starts at  $1e-2$  and then decays towards 0 using a cosine scheduler. During this evaluation, we do not apply any data augmentation.

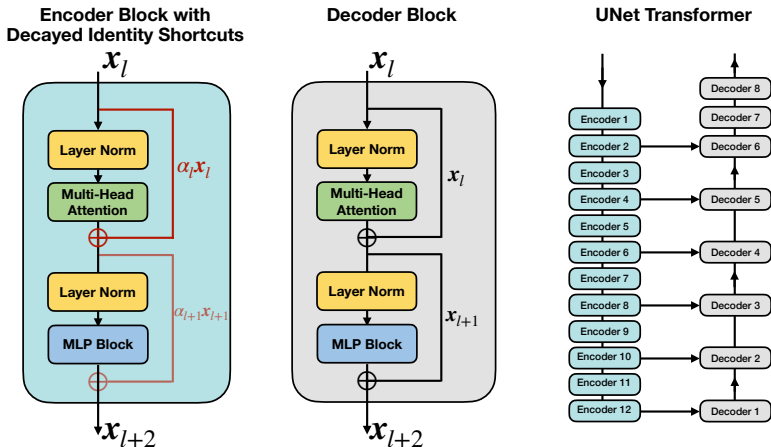


**Fig. 6:** We present our enhanced UNet Transformer architecture for Masked Auto-encoder. (1) **Left:** Our customized encoder blocks, equipped with our proposed decay identity shortcuts. (2) **Middle:** Standard transformer blocks as the decoder blocks. (3) **Right:** We incorporate the decay identity shortcuts exclusively within the encoder blocks of our UNet transformer and employ standard transformer blocks for the decoder. To support abstract representation learning at the bottleneck, *i.e.*, the last layer of the Encoder 12, we adopt the UNet [50] architecture and create skip connections that transmit every other encoder feature directly to the decoder.

Dataset	Backbone	$\alpha_{\min}$					
		0.5	0.6	0.7	0.8	0.9	1.0
ImageNet-1K	ViT-B/16	69.4	<b>72.3</b>	68.5	-	-	-
ImageNet-100	ViT-B/16	82.3	<b>83.6</b>	81.8	79.8	79.2	76.5
ImageNet-100	ViT-S/16	<b>78.6</b>	78.5	78.1	75.2	73.5	69.2

**Table 4: Linear probing accuracy of our method by varying  $\alpha_{\min}$ , the architecture size, and the dataset.** We extend the ablation studies detailed in Table. 2 by including linear probing results for the ImageNet-1K dataset. The results indicate that the most favorable  $\alpha_{\min}$  consistently falls within the range of [0.5, 0.6] for ImageNet-1K and ImageNet-100 experiments.

## 8.2 Modified Architecture

We present a visualization of our UNet transformer design, as outlined in Section 3.2, in Fig. 6. It’s important to note that decayed identity shortcuts are exclusively implemented within the encoder block. Additionally, we establish skip connections from alternating blocks in the encoder to the decoder, following the UNet [50] architecture’s design principles.

### 8.3 Further Ablation of Maximum Decay Rate on ImageNet-1K

We present the results of ablating the choices of  $\alpha_{\min}$  on ImageNet-1K dataset in Table.4. From the table, we show that the optimal  $\alpha_{\min}$  for ViT-B/16 on ImageNet-100 matches the optimal one for ImageNet-1K, while a lower  $\alpha_{\min}$  is preferred for a smaller architecture ViT-S/16.